IEEE Robotics and Automation Letters (RAL) paper presented at
2024 IEEE/RSJ International Conference on Intelligent Robots and Systems (IROS)
October 14-18, 2024. Abu Dhabi, UAE

Design Optimization of Wire Arrangement with Variable Relay Points in Numerical Simulation for Tendon-driven Robots

Kento Kawaharazuka[1], Shunnosuke Yoshimura[1], Temma Suzuki[1], Kei Okada[1], and Masayuki Inaba[1]

***Abstract*— One of the most important features of tendon-driven robots is the ease of wire arrangement and the degree of freedom it affords, enabling the construction of a body that satisfies the desired characteristics by modifying the wire arrangement. Various wire arrangement optimization methods have been proposed, but they have simplified the configuration by assuming that the moment arm of wires to joints are constant, or by disregarding wire arrangements that span multiple joints and include relay points. In this study, we formulate a more flexible wire arrangement optimization problem in which each wire is represented by a start point, multiple relay points, and an end point, and achieve the desired physical performance based on black-box optimization. We consider a multi-objective optimization which simultaneously takes into account both the feasible operational force space and velocity space, and discuss the optimization results obtained from various configurations.**

I. INTRODUCTION

A variety of tendon-driven robots have been constructed so far [1]–[3]. These have various advantages such as variable stiffness control [4] and robust response to wire breakage [5]. Among the advantages, we focus on the ease of wire arrangement and the degree of freedom it affords in this study. Compared to axis-driven robots, tendon-driven robots can freely select the start, relay, and end points of wires, and can easily construct bodies with various configurations [3]. By modifying the wire arrangement, it is possible to construct a body that satisfies the desired characteristics, and various wire arrangement design optimization methods have been proposed so far. [6] numerically optimizes muscle Jacobian and pulley radius for robot fingers to ensure a torque space equivalent to that of humans. [7] exploratively optimizes the distance between joints and wires to enlarge the feasible joint angle space for a continuum robot. [8] optimizes the spacing of fingers, wire pulley radius, and pulley spacing based on genetic algorithm for a two-fingered hand. [9] numerically optimizes the wire pulley radius, elasticity, and pretension for the design of asymmetric compliance actuators. [10] optimizes the wire attachment position for Cable-Driven Parallel Robots (CDPR) based on evolutionary algorithm. [11] numerically optimizes the tension and wire attachment position for CDPR to optimize its stiffness. [12] numerically optimizes the start and end point positions of muscles for a musculoskeletal robot with the attached link of each point fixed. [13] optimizes the presence or absence of moment arm of each muscle for each joint for a musculoskeletal robot with brute force search. [14] optimizes muscle Jacobian for a musculoskeletal robot by genetic algorithm.

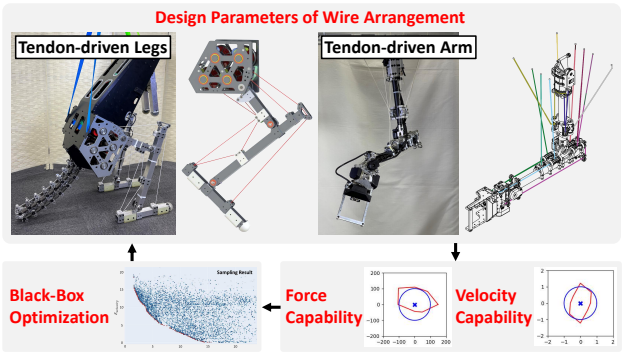

Fig. 1. The concept of this study. We prepare design parameters of wire arrangement, calculate the evaluation value for target and feasible force / velocity regions regarding each design, and obtain the design parameter with the best performance by multi-objective black-box optimization.

Here, the wire arrangement configuration is mainly divided into two types: a type with constant moment arm using pulleys [6], [8], [9], [13], [14], and a type in which the moment arm changes depending on the joint angle by expressing the wire route with its start, relay, and end points [7], [10]–[12]. Note that for the type with constant moment arm, the moment arm can be designed directly by the pulley radius, and it is easy to guarantee the moment arm at various joint angles, but the ease of wire arrangement is lost because it is difficult to obtain large moment arm due to the large pulleys placed at all joints. In terms of optimization methods, there are two types: those that deal mainly with continuous values and can be optimized analytically [6], [9], [11], [12], and those that use black-box optimization for discrete values or other complex settings [7], [8], [10], [13], [14].

On the other hand, these studies have either focused on optimizing constant moment arms or only the start and end points of wires, disregarding complex wire configurations that span multiple joints and include bends with various relay points. Also, research on complex optimization involving both continuous and discrete values from multiple objective functions is scarce. If we can explore the presence or absence of wire bends, links to which the relay points are attached, and changes in the attached positions, it should be possible to create body configurations that can appropriately perform a wider variety of tasks. Therefore, we propose a wire arrangement design optimization method that takes into account variable relay points. We perform multi-objective black-box optimization by setting up a problem in which each wire can freely choose which position of each link it passes through, and by setting the realization of target

[1] The authors are with the Department of Mechano-Informatics, Graduate School of Information Science and Technology, The University of Tokyo, 7-3-1 Hongo, Bunkyo-ku, Tokyo, 113-8656, Japan. [kawaharazuka, yoshimura, t-suzuki, k-okada, inaba]@jsk.t.u-tokyo.ac.jp

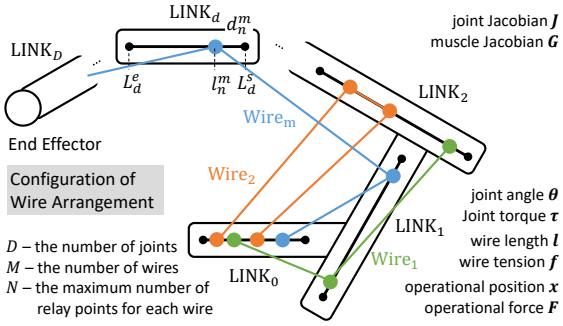

Fig. 2. The design parameters of wire arrangement. The number of wires M, the number of relay points N, the position of the relay point l_n^m, and the link d_n^m that the relay point is attached to are set as variables.

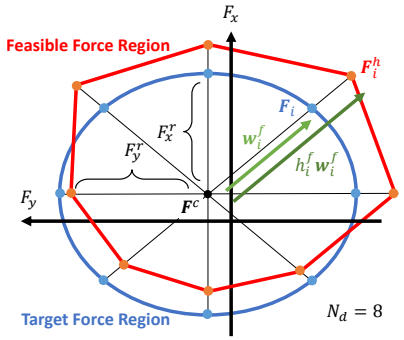

Fig. 3. The definition of variables for calculation of objective function for feasible operational force space.

operational force and velocity spaces as objective functions (Fig. 1). We show that various target operational force and velocity spaces can be realized by appropriately selecting the wire relay points, and discuss how the performance varies with the number of wires and relay points. We also show that the performance of this study is equivalent to or better than that of a configuration with constant moment arm using pulleys, while maintaining the degree of freedom of wire arrangement and large moment arm.

II. Design Optimization of Wire Arrangement with Variable Relay Points

First, we set discrete and continuous parameters for wire arrangement. Next, we define target operational force and velocity spaces, along with their corresponding objective functions. Lastly, we conduct multi-objective black-box optimization based on these design parameters and objectives.

A. Design Parameters of Wire Arrangement

In this study, the joint structure is predefined and only the wire arrangement is optimized. All motors and the start points of wires are located at the root of the robot. This structure maximizes the advantage of tendon-driven robots, in that the weight of the movable part can be reduced by separating the actuators and links. Note that the problem setting of this study is feasible in hardware, exemplified by the legs of the kangaroo robot [2] shown in Fig. 1.

An overview of the design parameters is shown in Fig. 2. We consider a robot with M wires for a given link structure with D joints. Let LINK$_0$ be the first link that the actuators are attached to, and LINK$_D$ be the last link. We set the end of LINK$_D$ as an end effector. Let N ($N \geq 2$) be the maximum number of relay points (including start and end points) for each wire. The n-th ($1 \leq n \leq N$) relay point on the m-th ($1 \leq m \leq M$) wire is attached to the link d_n^m ($0 \leq d_n^m \leq D$). The position of the relay point attached to the link is expressed as l_n^m ($0.0 \leq l_n^m \leq 1.0$). For simplicity, the relay points of LINK$_d$ ($0 \leq d \leq D$) are arranged in a straight line on the link, and the position is within $[L_d^s, L_d^e]$ ($L_d^{\{s,e\}}$ is a constant). That is, on LINK$_d$, $l_n^m = 0$ represents the position L_d^s, $l_n^m = 1$ represents the position L_d^e, and the actual link position is $L_d^s + l_n^m(L_d^e - L_d^s)$. The first relay point can be attached to only LINK$_0$, while the rest of the relay points can be attached to $LINK_d$ ($0 \leq d \leq D$). In summary, the design parameter of each wire m is a continuous value of l_1^m at $n = 1$, and a continuous value of l_n^m and a discrete value of d_n^m with $D + 1$ choices at $n \geq 2$.

As a comparison, we also perform experiments for the case with constant moment arm. The design parameters of each wire m are represented by continuous values of moment arm r_d^m ($0.0 \leq r_d^m \leq 1.0$) for each joint d. Let $[R_d^s, R_d^e]$ denote the range of possible moment arms at each joint d, $r_d^m = 0$ represents the radius R_d^s, $r_d^m = 1$ represents the radius R_d^e, and the actual moment arm is $R_d^s + r_d^m(R_d^e - R_d^s)$. As described in Section I, while this configuration has high performance because the moment arm can be designed directly, the ease of wire arrangement is lost and the large moment arm becomes difficult to obtain.

B. Calculation of Objective Functions

Objective functions are calculated for the obtained designs. In this study, we use feasible operational force space (OFS) and operational velocity space (OVS) as the objective functions. We define the target OFS and OVS, and find design solutions that realize them as much as possible. We consider OFS and OVS in a two-dimensional (2D) plane, but this can be extended to three dimensions (3D) in a similar manner.

First, some basic formulas are described. Let $\boldsymbol{f}$ be wire tension, $\boldsymbol{\tau}$ be joint torque, and $\boldsymbol{F}$ be operational force of the end effector. Also, let $\boldsymbol{l}$ be wire length, $\boldsymbol{\theta}$ be joint angle, and $\boldsymbol{x}$ be operational position of the end effector. Here, the following relations generally hold,

$$\boldsymbol{l} = \boldsymbol{g}_m(\boldsymbol{\theta}) \tag{1}$$
$$\dot{\boldsymbol{l}} = \boldsymbol{G}(\boldsymbol{\theta})\dot{\boldsymbol{\theta}} \tag{2}$$
$$\boldsymbol{\tau} = -\boldsymbol{G}^T(\boldsymbol{\theta})\boldsymbol{f} \tag{3}$$
$$\boldsymbol{x} = \boldsymbol{g}_j(\boldsymbol{\theta}) \tag{4}$$
$$\dot{\boldsymbol{x}} = \boldsymbol{J}(\boldsymbol{\theta})\dot{\boldsymbol{\theta}} \tag{5}$$
$$\boldsymbol{\tau} = \boldsymbol{J}^T(\boldsymbol{\theta})\boldsymbol{F} \tag{6}$$

where $\boldsymbol{g}_m$ denotes the mapping from $\boldsymbol{\theta}$ to $\boldsymbol{l}$ and $\boldsymbol{g}_j$ denotes the mapping from $\boldsymbol{\theta}$ to $\boldsymbol{x}$. Also, $\boldsymbol{G}$ denotes the muscle Jacobian and $\boldsymbol{J}$ denotes the joint Jacobian. The minimum and maximum values of wire tension $\boldsymbol{f}$ are denoted by $\boldsymbol{f}^{min}$ and $\boldsymbol{f}^{max}$, and those of wire velocity $\dot{\boldsymbol{l}}$ are denoted by $\dot{\boldsymbol{l}}^{min}$ and $\dot{\boldsymbol{l}}^{max}$. In this study, we do not change the ranges dynamically by considering back electromotive force.

Next, we describe the objective function for the feasible OFS (Fig. 3). Defining the target OFS in a 2D plane as an ellipse, its parameters are the center point of the ellipse $\boldsymbol{F}^c = \begin{pmatrix} F_x^c & F_y^c \end{pmatrix}^T$ and the radius of the ellipse for the x- and y-axes $F^r_{\{x,y\}}$. Note that the feasible OFS and OVS are always convex. When this ellipse is divided into N_d pieces, the operational force $\boldsymbol{F}_i$ at each point i ($0 \leq i < N_d$) on the ellipse can be expressed as follows.

$$\boldsymbol{w}_i^f := \begin{pmatrix} F_x^r \cos(2\pi i/N_d) \\ F_y^r \sin(2\pi i/N_d) \end{pmatrix} \tag{7}$$

$$\boldsymbol{F}_i := \boldsymbol{w}_i^f + \boldsymbol{F}^c \tag{8}$$

Here, for each point i, we introduce a value h_i^f that expresses by how much the feasible OFS exceeds the target OFS, and define the following point $\boldsymbol{F}_i^h$.

$$\boldsymbol{F}_i^h := h_i^f \boldsymbol{w}_i^f + \boldsymbol{F}^c \tag{9}$$

We maximize h_i^f by the following linear programming.

$$\underset{h_i^f, \boldsymbol{f}}{\text{maximize}} \quad h_i^f \tag{10}$$

$$\text{subject to} \quad -\boldsymbol{G}^T(\boldsymbol{\theta})\boldsymbol{f} = \boldsymbol{J}^T(\boldsymbol{\theta})\boldsymbol{F}_i^h \tag{11}$$

$$\boldsymbol{f}^{min} \leq \boldsymbol{f} \leq \boldsymbol{f}^{max} \tag{12}$$

When $h_i^f = 1$, the target and feasible OFS coincide for the direction $\boldsymbol{w}_i^f$, and $h_i^f \geq 1$ should be satisfied. Therefore, we compute h_i^f for each point i, set the following E_{force} as the objective function, and minimize it.

$$E_{force} := \sum_i \max(1 - h_i^f, 0) \tag{13}$$

If gravity compensation is considered, $\boldsymbol{F}^c$ should be obtained by the following quadratic programming,

$$\underset{\boldsymbol{F}^c}{\text{minimize}} \quad ||\boldsymbol{F}^c||_2^2 \tag{14}$$

$$\text{subject to} \quad \boldsymbol{\tau}_g = \boldsymbol{J}^T(\boldsymbol{\theta})F^c \tag{15}$$

where $\boldsymbol{\tau}_g$ is the gravity compensation torque required at the current joint angle $\boldsymbol{\theta}$ and $||\cdot||_2$ is the L2 norm. Note that in practice, since $\boldsymbol{J}^T(\boldsymbol{\theta})\boldsymbol{F}^c = \boldsymbol{\tau}_g$ in Eq. 11, the calculation of $\boldsymbol{F}_c$ is not necessary for optimization, but only for drawing the elliptic center.

Next, we describe the objective function for the feasible OVS. Defining the target OVS in a 2D plane as an ellipse, its parameters are the radius $v^r_{\{x,y\}}$ of the ellipse for the x- and y-axes. When this ellipse is divided into N_d pieces, the operational velocity $\boldsymbol{v}_i$ at each point i ($0 \leq i < N_d$) on the ellipse can be expressed as follows.

$$\boldsymbol{w}_i^v := \begin{pmatrix} v_x^r \cos(2\pi i/N_d) \\ v_y^r \sin(2\pi i/N_d) \end{pmatrix} \tag{16}$$

$$\boldsymbol{v}_i := \boldsymbol{w}_i^v \tag{17}$$

Here, for each point i, we introduce a value h_i^v that expresses by how much the feasible OVS exceeds the target OVS, and define the following point $\boldsymbol{v}_i^h$.

$$\boldsymbol{v}_i^h := h_i^v \boldsymbol{w}_i^v \tag{18}$$

We maximize h_i^v by the following linear programming.

$$\underset{h_i^v, \dot{\boldsymbol{\theta}}}{\text{maximize}} \quad h_i^v \tag{19}$$

$$\text{subject to} \quad \boldsymbol{J}(\boldsymbol{\theta})\dot{\boldsymbol{\theta}} = \boldsymbol{v}_i^h \tag{20}$$

$$\dot{\boldsymbol{l}}^{min} \leq \boldsymbol{G}(\boldsymbol{\theta})\dot{\boldsymbol{\theta}} \leq \dot{\boldsymbol{l}}^{max} \tag{21}$$

Similarly to E_{force}, we set the following $E_{velocity}$ as the objective function, and minimize it.

$$E_{velocity} := \sum_i \max(1 - h_i^v, 0) \tag{22}$$

Note that we can define target spaces of various shapes other than ellipsoids, and can freely define various objective functions such as operational wrench force or rotation velocity.

C. Design of Wire Arrangement Using Multi-Objective Black-Box Optimization

We have formulated the design parameters and the objective functions. By using them, multi-objective optimization is performed to determine the design parameters. In this study, we use NSGA-II, a multi-objective optimization method implemented in optuna [15], a black box optimization library. NSGA-II was chosen for its ability to perform multi-objective optimization, handle both continuous and discrete parameters, and handle a relatively large number of samples. Note that if no solution is found for the linear programming problem in Eq. 10–Eq. 12 or Eq. 19–Eq. 21, the design is pruned. In the experiments, we illustrate the obtained Pareto solutions with N_{sample} as the number of samples, and discuss the wire arrangement and the feasible OFS and OVS of the design. Although only two objective functions are used, multi-objective optimization is also possible by using other objective functions such as minimizing the wire length to suppress elongation or adding constraints on the number and positions of relay points.

III. Experiments

The experimental setup is shown in Fig. 4. We focus on a two-joint and three-link mechanism in a 2D plane for detailed experiments and comparisons. The robot model used in this study is shown under "Robot Configuration" in Fig. 4, where LINK_0 has a length of 0.4 m and $\text{LINK}_{\{1,2\}}$ has a length of 0.6 m. Relay points can be attached to any of three links from one end to the other. LINK_0 is fixed and the weight of $\text{LINK}_{\{1,2\}}$ is set to 4 kg assuming the density of aluminum. The total value of $E_{\{force,velocity\}}$ for the four joint angles (①–④) is used as the actual objective function, where the angle of each joint is changed by 15 deg as shown under "Evaluated Joint Angles" in Fig. 4. Note that we have chosen this configuration for reasons of computational complexity, visualization, and the desire to emphasize significant changes in joint Jacobian due to the change in $\boldsymbol{\theta}_1 + \boldsymbol{\theta}_2$, though a wider range of joint angle states should be considered. As a comparison, several experiments are conducted by changing the design parameters and settings. First, as shown under "Design Parameters" in Fig. 4, we conduct experiments for two types: **Variable** in which each relay point can be freely

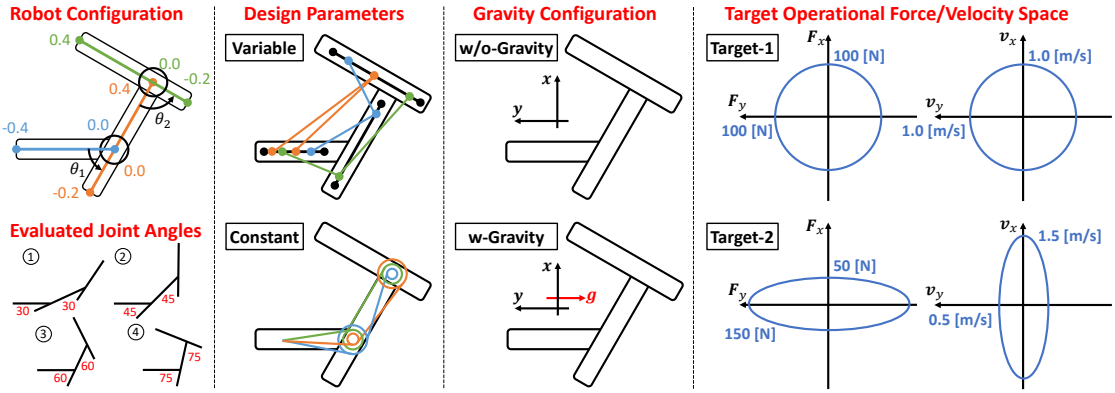

Fig. 4. The experimental setup of this study. The robot configuration for $L_d^{\{s,e\}}$ and the evaluated joint angles are shown. The design parameters were changed to **Variable** or **Constant**, gravity configuration to **w/o-Gravity** or **w-Gravity**, and target operational force / velocity space to **Target-1** or **Target-2**.

selected, and **Constant** in which the muscle Jacobian is kept constant using pulleys. In this comparison, we vary the number of wires M and the maximum number of relay points N. For **Constant**, the range of moment arms of the wire for each joint is set to $[R_d^s, R_d^e]$=[-0.1, 0.1] [m] (since the distance between the joints is 0.4 m, the moment arm can be increased to 0.2, but we set it to 0.1 based on the feasibility. In some experiments, we set [-0.4, 0.4] [m] in order to investigate the maximum possible performance). We also compare two types: **w/o-Gravity** which is not affected by gravity, and **w/-Gravity** which is affected by gravity as in the human arm as shown under "Gravity Configuration". In addition, as shown under "Target Operational Force/Velocity Space", we perform experiments by setting types of target OFS and OVS: **Target-1** and **Target-2**. For other parameters, we set $f^{min} = 10$ [N], $f^{max} = 200$ [N], $\dot{l}^{min} = -0.4$ [m/s], $\dot{l}^{max} = 0.4$ [m/s], $N_d = 8$, and $N_{sample} = 10000$ (the performance is equivalent to that of a Maxon 90W BLDC motor with 29:1 gear ratio). For each experiment, the sampling results and Pareto solutions are shown, and the target space (blue lines) and the feasible space (red lines) of force and velocity are shown for the design with the smallest $|E_{force} - E_{velocity}|$ (the solution in which E_{force} and $E_{velocity}$ are considered equally). For **Variable**, its wire arrangement is shown as a figure, and for **Constant**, the moment arm of each wire for each joint is shown since the wire arrangement is difficult to visualize.

A. *Target-1 w/o Gravity*

We show the experimental results for **Target-1** and **w/o-Gravity**. For **Variable**, the parameters are varied as $M = \{3, 4\}$ and $N = \{2, 3\}$. For **Constant**, the parameters are varied as $M = \{3, 4\}$. The results are shown in Fig. 5.

First, we explain how to interpret the results by referring to the example of **Variable** when $M = 3$ and $N = 2$. The upper left figure shows the sampling result of optimization, where E_{force} is for the x-axis and $E_{velocity}$ is for the y-axis. The further down to the left of the sampling result graph, the better the solution becomes. Among the sampling results, the samples represented by the red dots are the Pareto solutions. The solution with the smallest $|E_{force} - E_{velocity}|$ is indicated by a red circle, and $(E_{force}, E_{velocity})$ and its wire arrangement are shown. As $M = 3$, there are three wires, and as $N = 2$, there are two relay points, a start point and an end point. Below the figures, the target and feasible OFS and OVS of this design for ①–④ in Fig. 4 are shown with $F_{\{x,y\}}$ or $v_{\{x,y\}}$ as $\{x, y\}$-axes. If the feasible space (red line) exceeds the target space (blue line), $E_{\{force,velocity\}}$ becomes smaller.

Second, we discuss the overall characteristics of the experiment. Since it is possible to increase the operational velocity by keeping the moment arm as small as possible, there is almost certain to be a sampling at $E_{velocity} = 0$. On the other hand, there are many cases where there is no sampling with $E_{force} = 0$, because the moment arm has a maximum value. For example, for **Variable** with $N = 2$, or for **Constant**, there is no sampling at $E_{force} = 0$. In particular, E_{force} is much larger for **Constant** than for **Variable** because it is difficult for **Constant** to obtain large moment arm (this will be analyzed in detail in the next experiment). OFS and OVS show that the velocity takes large values, while the force takes relatively small values. Next, $E_{\{force,velocity\}}$ tends to be smaller as the number of wires and relay points increase. The larger the number of wires and relay points, the wider the design range becomes, and the more flexibly the target OFS and OVS can be covered. For this experimental setting, it is found that increasing the number of relay points is more effective than increasing the number of wires. When $N = 2$, the feasible OFS and OVS cannot be brought close to the target space, and the feasible space is sharp in a certain direction. On the other hand, when $N = 3$, it is found that the feasible OFS and OVS are round and close to the target space. As for the wire arrangement, when $N = 2$ for both $M = 3$ and $M = 4$, there exist wires that control the first and second joints independently, as well as a wire that controls the two joints simultaneously (to control the second joint independently, the start point of that wire is placed near the first joint at LINK_0). On the other hand, when $N = 3$, there are multiple wires that control two joints simultaneously, and we can see diverse wire arrangements.

Third, a detailed analysis is given for **Constant**. We relax the restrictions of $R_d^{\{s,e\}}$ in Fig. 5 and show the results when $[R_d^s, R_d^e]$=[-0.4, 0.4], which is not feasible in practice. This allows us to compare **Variable** and **Constant** without design

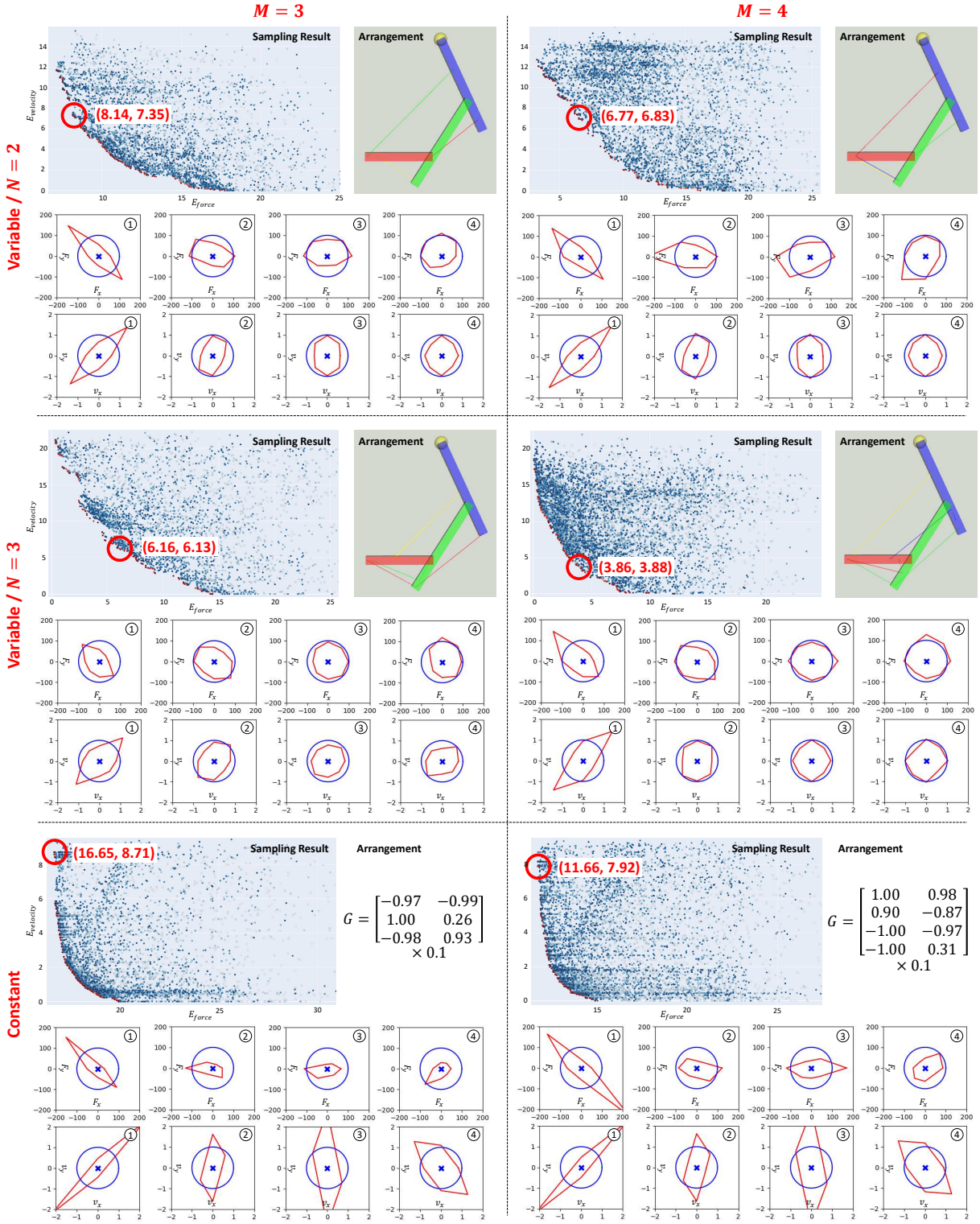

Fig. 5. The experiment of Target-1 w/o Gravity. For **Variable** with $M = \{3, 4\}$ and $N = \{2, 3\}$ and for **Constant** with $M = \{3, 4\}$, the sampling results and Pareto solutions are shown. For one Pareto solution with minimized $|E_{force} - E_{velocity}|$, the wire arrangement and target (blue line) and feasible (red line) operational force / velocity spaces are shown.

restrictions. Here, we limit the evaluated joint angles to ① and ④ (the reason will be described later), and **Variable** with $N = \{4, 5, 6\}$ and $M = 4$ is considered for comparison. Note that we set $N_{sample} = 50000$ for this experiment because the number of parameters is much larger than in Fig. 5. The results are shown in Fig. 6. It can be seen that for **Variable**, better solutions are generated as N is increased. For the solution with the smallest $|E_{force} - E_{velocity}|$, the performance of **Variable** with $N = 5$ is almost equal to that of **Constant**. In other words, for **Constant**, performance without restrictions is much higher than that with restrictions. Moreover, by increasing N for **Variable**, we can obtain

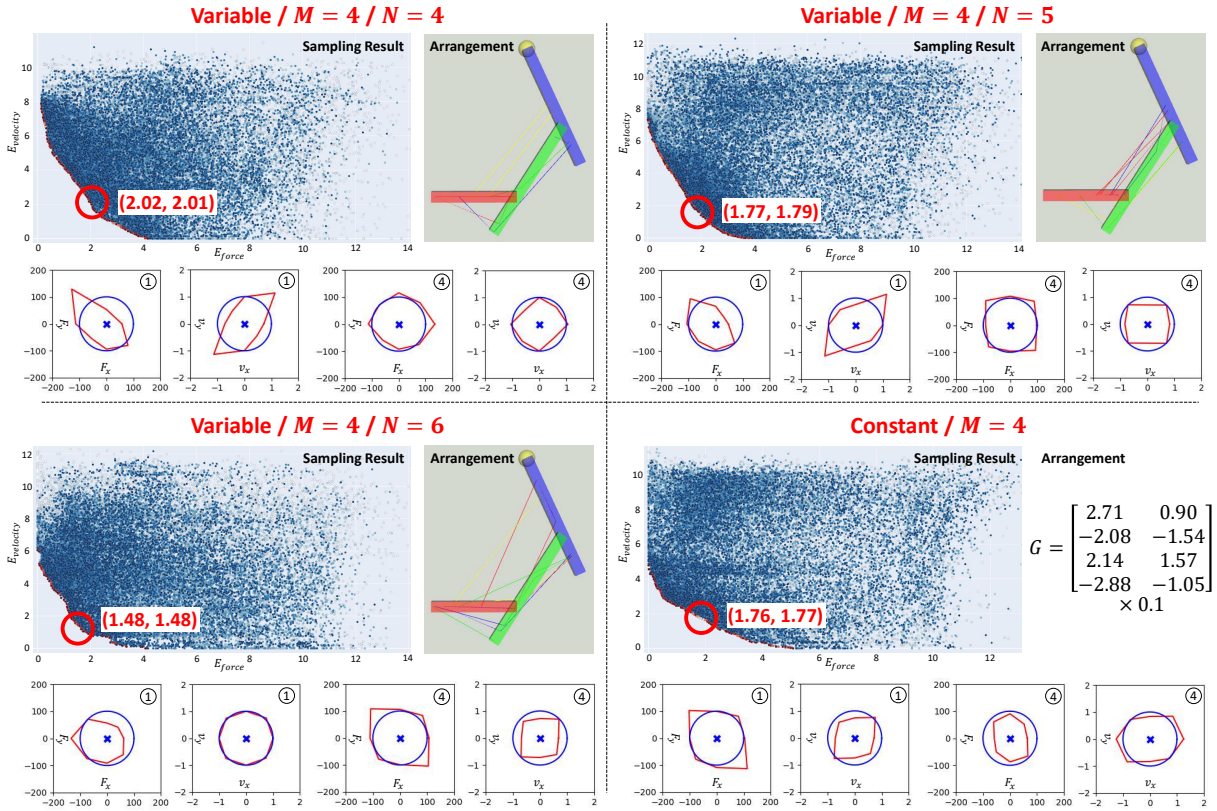

Fig. 6. The detailed analysis of **Constant** without restrictions for Target-1 w/o Gravity. For **Variable** with $M = 4$ and $N = \{4, 5, 6\}$ and for **Constant** with $M = 4$, the sampling results and Pareto solutions are shown.

higher performance than that of **Constant**. This is because the same $\boldsymbol{G}$ is used for each joint angle for **Constant**, while different $\boldsymbol{G}$ is used for each joint angle for **Variable**. On the other hand, the performance of **Variable** is not as good as or better than that of **Constant** unless the number of relay points is considerably increased, as in $N = \{5, 6\}$. In this experiment, the evaluated joint angles are limited to ① and ④, which differ greatly in $\boldsymbol{J}$. If the evaluated joint angles are increased to ①–④, it is difficult to form $\boldsymbol{G}$ that is appropriate for all of ①–④, and even if $\boldsymbol{G}$ is always constant or even if $\boldsymbol{G}$ is varied, the performance does not change significantly. Therefore, even when N is increased, there is no significant difference between **Constant** and **Variable**.

B. Target-1 w/ Gravity

We show the experimental results for **Target-1** and **w/-Gravity**. We compare the results between **w/o-Gravity** and **w/-Gravity** for **Variable** with $M = 4$ by changing the parameters as $N = \{2, 3\}$. We limit the evaluated joint angles to ② and ③ for this experiment (the reason will be described later). The results are shown in Fig. 7. The performance of the solutions increases by increasing N, or with the presence of gravity. In particular, the sampling results show that the presence of gravity does not significantly change the minimum value of E_{force}, but $E_{velocity}$ becomes smaller overall. Gravity always exerts a force in the negative direction on the y-axis. In the current setup of feasible wire arrangement, the force in the positive direction on the y-axis is easily exerted, but the force in the negative direction is hardly exerted and can be compensated by gravity. In this experiment, the evaluated joint angles are limited to ② and ③, which have similar $\boldsymbol{J}$. If the evaluated joint angles are increased to ①–④, the difficulty in forming appropriate $\boldsymbol{G}$ for all the joint angles increases, and the performance difference between **w/o-Gravity** and **w-Gravity** becomes smaller.

C. Target-2 w/o Gravity

We show the experimental results for **Target-2** and **w/o-Gravity**. We perform comparative experiments for **Variable** by changing the parameters as $M = \{3, 4\}$ and $N = \{2, 3\}$. The results are shown in Fig. 8. It can be seen that the performance of the obtained solutions becomes higher by increasing M or N. However, increasing N does not significantly change the performance as in Fig. 5. Compared to **Target-1**, for **Target-2**, the increase in M causes a larger change in performance than an increase in N. From the result for $N = 3$ and $M = 4$, the feasible OFS and OVS can realize the sharp target spaces well.

IV. Discussion

The experimental results are summarized and discussed. First, the multi-objective optimization of this study has allowed us to obtain a variety of Pareto solutions where a trade-off exists to achieve the target OFS or OVS. It is found that the performance of the solution is improved by increasing the number of wires or the number of relay points for **Variable**. Whether it is better to increase the

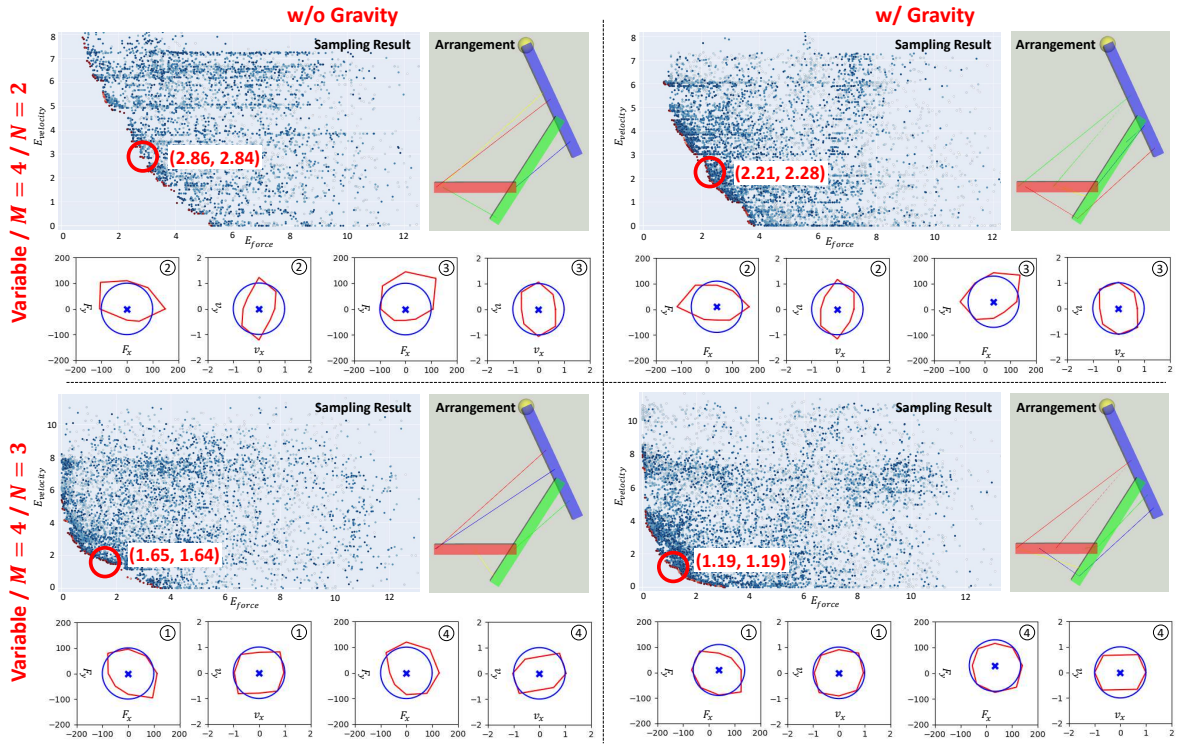

Fig. 7. The experiment of Target-1 w/ Gravity. For **Variable** with $M = 4$, $N = \{2, 3\}$, and {**w/o-Gravity**, **w/-Gravity**}, the sampling results and Pareto solutions

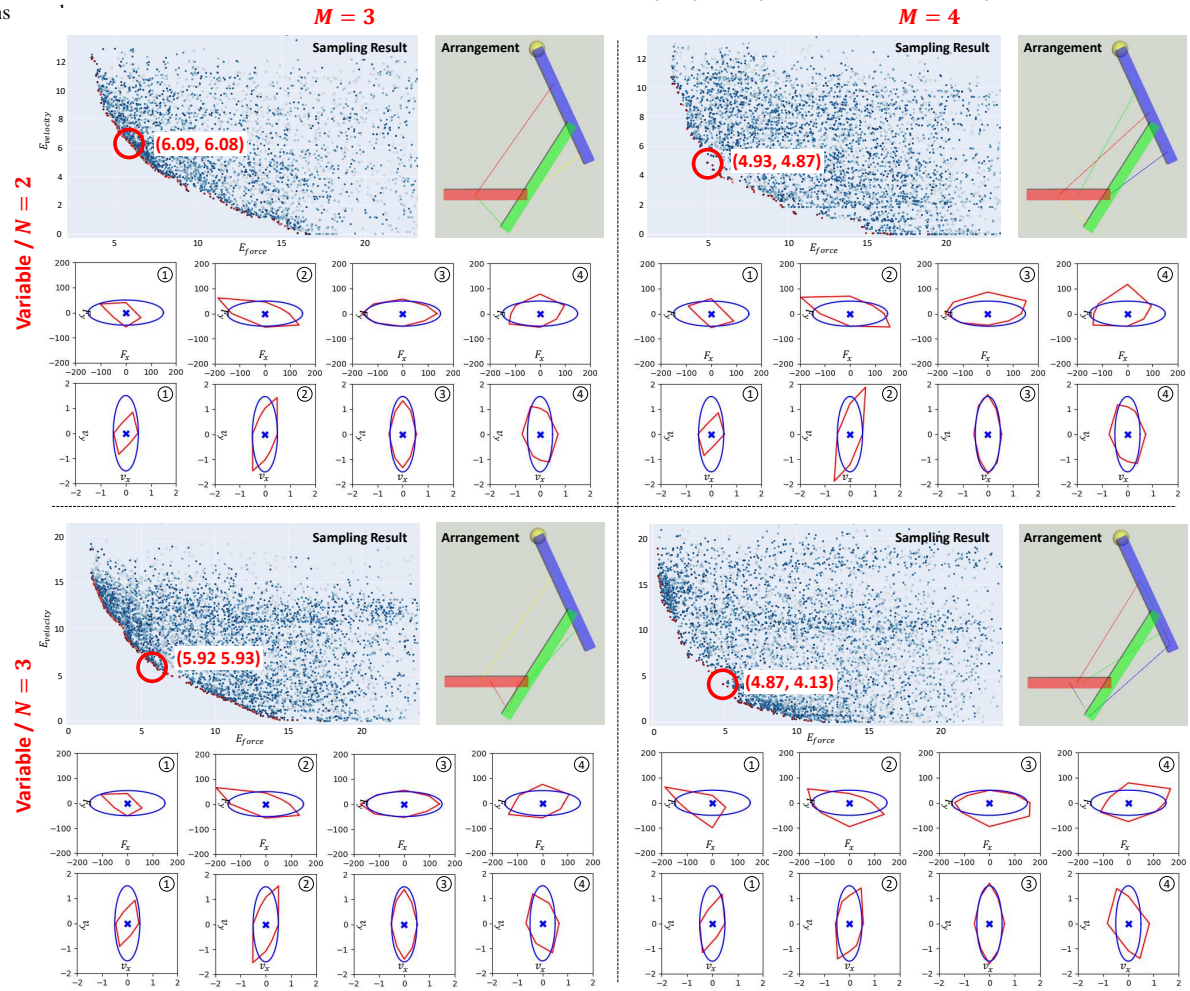

Fig. 8. The experiment of Target-2 w/o Gravity. For **Variable** with $M = \{3, 4\}$ and $N = \{2, 3\}$, the sampling results and Pareto solutions are shown.

number of wires or the number of relay points depends on the geometry of the target OFS and OVS. Additionally, the performance of **Constant** is inferior to that of **Variable**, because **Constant** cannot have large moment arm. On the other hand, by removing the restrictions of the moment arm, higher performance can be obtained. Since **Constant** uses the same $\boldsymbol{G}$ for all joint angles, **Variable** theoretically has better performance as it can change $\boldsymbol{G}$ according to the joint angle. However, in order for **Variable** to achieve higher performance than that of **Constant** without restrictions, it is necessary to significantly increase the number of relay points. This implies that a large degree of freedom in wire arrangement is necessary to make $\boldsymbol{G}$ nonlinear enough to accommodate changes in $\boldsymbol{J}$ at each joint angle. Note that by increasing the gear ratio of the motor, **Constant** can achieve high performance without relaxing the restrictions, but at the cost of backdrivability. For **Variable**, there is also a trade-off that the friction at the pulleys should increase as the number of relay points increases. In addition, the effect of gravity may have a positive effect depending on the setting. The wire drive can produce anisotropic torque depending on the direction of joint rotation, and so gravity can be used effectively in many cases.

We discuss future issues. First, the design parameters of the manipulator in this study were relatively simple because we handled a planar manipulator. When the manipulator becomes 3D, it is necessary to take into account the interference of wires during movement, which requires a more complicated formulation. In addition, the joint structure is not optimized in this study. Although simultaneous optimization of link lengths with wire arrangements can be performed in the same framework, the design parameter space becomes huge when closed links and branching of links are considered. Furthermore, it should be noted that aspects such as wire elongation and friction are not addressed in this study. Second, although we have considered the feasible OFS and OVS as the objective function in this study, this framework can flexibly consider a wider variety of objective functions. In the future, it is necessary to consider more complex and realistic settings for objective functions in accordance with the actual tasks to be realized. In addition, we would like to develop a tendon-driven robot that actually implements the obtained solution, and confirm its effectiveness.

V. CONCLUSION

We proposed a design optimization method for wire arrangement in a tendon-driven robot with variable relay points. While previous studies have focused on conditions with constant moment arm or fixed links to attach relay points to, this study deals with a broader problem and performs multi-objective black-box optimization aiming at achieving a target operational force space and velocity space. Various designs can be represented by setting the links each wire attaches to and the positions of the relay points as variables. A body using variable relay points can be designed more freely in terms of its physical capabilities compared to a general tendon-driven robot with constant moment arm using pulleys. We expect that this concept will be a key to solving various wire arrangement design problems.

REFERENCES

[1] G. Endo, A. Horigome, and A. Takata, "Super Dragon: A 10-m-Long-Coupled Tendon-Driven Articulated Manipulator," *IEEE Robotics and Automation Letters*, vol. 4, no. 2, pp. 934–941, 2019.

[2] S. Yoshimura, T. Suzuki, M. Bando, S. Yuzaki, K. Kawaharazuka, K. Okada, and M. Inaba, "Design Method of a Kangaroo Robot with High Power Legs and an Articulated Soft Tail," in *Proceedings of the 2023 IEEE/RSJ International Conference on Intelligent Robots and Systems*, 2023.

[3] K. Kawaharazuka, S. Makino, K. Tsuzuki, M. Onitsuka, Y. Nagamatsu, K. Shinjo, T. Makabe, Y. Asano, K. Okada, K. Kawasaki, and M. Inaba, "Component Modularized Design of Musculoskeletal Humanoid Platform Musashi to Investigate Learning Control Systems," in *Proceedings of the 2019 IEEE/RSJ International Conference on Intelligent Robots and Systems*, 2019, pp. 7294–7301.

[4] H. Kobayashi, K. Hyodo, and D. Ogane, "On Tendon-Driven Robotic Mechanisms with Redundant Tendons," *The International Journal of Robotics Research*, vol. 17, no. 5, pp. 561–571, 1998.

[5] K. Kawaharazuka, M. Nishiura, Y. Toshimitsu, Y. Omura, Y. Koga, Y. Asano, K. Okada, K. Kawasaki, and M. Inaba, "Robust Continuous Motion Strategy Against Muscle Rupture using Online Learning of Redundant Intersensory Networks for Musculoskeletal Humanoids," *Robotics and Autonomous Systems*, vol. 152, pp. 1–14, 2022.

[6] N. S. Pollard and R. C. Gilbert, "Tendon arrangement and muscle force requirements for human-like force capabilities in a robotic finger," in *Proceedings of the 2002 IEEE International Conference on Robotics and Automation*, 2002, pp. 3755–3762.

[7] P. Berthet-Rayne and K. Leibrandt and K. Kim and C. A. Seneci and J. Shang and G. Yang, "Rolling-joint design optimization for tendon driven snake-like surgical robots," in *Proceedings of the 2018 IEEE/RSJ International Conference on Intelligent Robots and Systems*, 2018, pp. 4964–4971.

[8] H. Dong, E. Asadi, C. Qiu, J. Dai, and I. Chen, "Geometric design optimization of an under-actuated tendon-driven robotic gripper," *Robotics and Computer-Integrated Manufacturing*, vol. 50, pp. 80–89, 2018.

[9] W. Roozing, Z. Li, D. G. Caldwell, and N. G. Tsagarakis, "Design Optimisation and Control of Compliant Actuation Arrangements in Articulated Robots for Improved Energy Efficiency," *IEEE Robotics and Automation Letters*, vol. 1, no. 2, pp. 1110–1117, 2016.

[10] I. B. Hamida, M. A. Laribi, A. Mlika, L. Romdhane, S. Zeghloul, and G. Carbone, "Multi-Objective optimal design of a cable driven parallel robot for rehabilitation tasks," *Mechanism and Machine Theory*, vol. 156, pp. 1–24, 2021.

[11] H. Jamshidifar, A. Khajepour, B. Fidan, and M. Rushton, "Kinematically-Constrained Redundant Cable-Driven Parallel Robots: Modeling, Redundancy Analysis, and Stiffness Optimization," *IEEE/ASME Transactions on Mechatronics*, vol. 22, no. 2, pp. 921–930, 2017.

[12] S. Zhong, J. Zhou, and W. Wu, "Constructing Constraint Force Field in Musculoskeletal Robot by Co-optimizing Muscle Arrangements and Constant Activations," in *2022 International Joint Conference on Neural Networks*, 2022, pp. 1–7.

[13] T. Asaoka, M. Kawamura, S. Kumakura, and I. Mizuuchi, "Determining the optimal multiarticular muscle arrangement of a musculoskeletal robot for a specific motion using dynamics simulation," in *Proceedings of the 2012 IEEE-RAS International Conference on Humanoid Robots*, 2012, pp. 216–221.

[14] K. Kawaharazuka, Y. Toshimitsu, M. Nishiura, Y. Koga, Y. Omura, Y. Asano, K. Okada, K. Kawasaki, and M. Inaba, "Design Optimization of Musculoskeletal Humanoids with Maximization of Redundancy to Compensate for Muscle Rupture," in *Proceedings of the 2021 IEEE/RSJ International Conference on Intelligent Robots and Systems*, 2021, pp. 3204–3210.

[15] T. Akiba, S. Sano, T. Yanase, T. Ohta, and M. Koyama, "Optuna: A Next-generation Hyperparameter Optimization Framework," in *Proceedings of the 25th ACM SIGKDD International Conference on Knowledge Discovery and Data Mining*, 2019.